INTERNATIONAL JOURNAL FOR NUMERICAL METHODS IN FLUIDS, VOL. 20, 1061–1080 (1995)

# A SPLIT-CHARACTERISTIC BASED FINITE ELEMENT MODEL FOR THE SHALLOW WATER EQUATIONS

O. C. ZIENKIEWICZ

*Institute of Numerical Methods in Engineering, University College of Swansea, Swansea SA2 8PP, U.K.*

AND

P. ORTIZ

*Centro de Estudios de Técnicas Aplicadas, Cedex, Alfonso XII, 3, E-28014 Madrid, Spain*

SUMMARY

A new algorithm for the solution of the shallow water equations is introduced. The formulation is founded on a suitable operator-splitting procedure for which a characteristic-based rational form of including balancing dissipation terms is achieved.

In the semi-explicit form the method circumvents the requirement of a critical time step given in terms of the wave celerity, which is restrictive for the analysis of long-wave propagation in shallow waters.

In this work the robustness of the algorithm is illustrated for transient shallow water problems and for some supercritical flows, where the choice of an algorithm with optimal diffusion properties is manifest.

KEY WORDS computational fluid dynamics; shallow water equations; tides

## 1. INTRODUCTION

The application of the finite element method to the solution of shallow water equations has an extensive development, shown by a substantial literature with some relevant publications by Lynch and Gray,[1] Peraire *et al.*,[2] Zienkiewicz *et al.*,[3] Kawahara *et al.*[4] and others.[5–8]

The remarkable contribution of the Taylor–Galerkin[9] and characteristic–Galerkin[10] methodologies for the finite element method in the field of compressible, high-speed flow problems has also been extended to the solution of the shallow water equations.[2]

However, while the Taylor–Galerkin method could be used for a general form of conservation equations with multiple characteristic speeds, only the characteristic–Galerkin method, proved for a single characteristic speed, justifies the use of Galerkin spatial discretization.[10]

The basis of the algorithm introduced in this work is essentially the fractional step procedure,[11] which has been successfully applied to incompressible flows (e.g. Reference 12) and more recently to compressible and incompressible flows in a unified formulation.[13,14]

The fractional step methodology exploited here allows a single characteristic velocity (the actual velocity) to be considered by the characteristic–Galerkin method. This gives a rational definition of the balancing dissipation terms and justifies the application of a Galerkin spatial discretization in the convective equation.[10,13]

CCC 0271–2091/95/091061–20

The semi-implicit form of the general formulation provides a critical time step dependent only on the current velocity, $\Delta t = h/u$, where $h$ is the element size and $u$ is the flow velocity, instead of a critical time step in terms of the wave celerity $c$, which places a severe constraint on fully explicit methods such as the Taylor–Galerkin approximation.[15]

The present method computes, as in the fractional step procedure, the pressure (or elevations of the free surface) by means of a Laplacian-type equation, whose self-adjointness makes the Galerkin space discretization optimal.

Otherwise, velocities are computed in two stages explicitly with the characteristic–Galerkin method, first considering the momentum equations ommiting the pressure gradient terms and finally with a correction coming from the computed new pressure.

A convenient form of the governing shallow water equations, depth-integrated assuming hydrostatic pressure distribution and constant horizontal velocities in depth, is described in the next section.

The subsequent sections are devoted to the discussion of the numerical solution proposed and to the application of the model to transient shallow water problems such as tidal lows and bore propagation and to steady subcritical and supercritical channel flows (including 'jumps' or shock patterns in the latter).

## 2. GOVERNING EQUATIONS

The shallow water equations in their depth-integrated form can be written in a Cartesian system $x_i$ ($i = 1, 2$) of space co-ordinates (see Figure 1), using the summation convention, as

$$\frac{\partial h}{\partial t} + \frac{\partial U_i}{\partial x_i} = 0 \quad (i = 1, 2), \tag{1}$$

$$\frac{\partial U_i}{\partial t} + \frac{\partial F_{ij}}{\partial x_j} + \frac{\partial p}{\partial x_i} + \frac{\partial G_{ij}}{\partial x_j} + Q_i = 0 \quad (i, j = 1, 2), \tag{2}$$

where $h = H + \eta$ and $U_i = hu_i$ are the unknowns. In the above $h$ is the total height of water, $H = H(x_1, x_2)$ the depth of water and $\eta$ the surface elevation with respect to the mean water level and $u_i$ are the depth-averaged components of the horizontal velocity.

$F_{ij} = hu_iu_j = U_iu_j$ is the $i$th component of the $j$th flux vector and $\mathbf{G}$ represents the diffusive, viscous, fluxes. Here the 'pressure' $p$ is defined as

$$p = \tfrac{1}{2}g(h^2 - H^2) \tag{3}$$

to maintain the analogy with equations of compressible flows.

The vector $\mathbf{Q}$ contains the source terms, which in general can be specified as

$$Q_i = -g(h - H)\frac{\partial H}{\partial x_i} + g\frac{u_i|u|}{C^2h} + r_i - \tau_i + \frac{h}{\rho}\frac{\partial p_a}{\partial x_i} \quad (i = 1, 2), \tag{4}$$

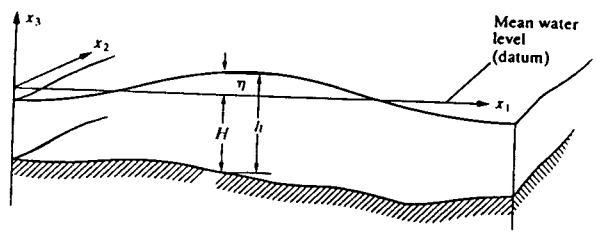


Figure 1. The shallow water problem notation

where the well-known Chezy–Manning formula is adopted for the bottom friction term, $r_i$ is the $i$th component of the Coriolis force

$$\mathbf{r} = \begin{bmatrix} -fu_2 \\ fu_1 \end{bmatrix},$$

with $f$ the Coriolis parameter, $\tau_i$ are the surface wind tractions, $\rho$ is the density of the water and $p_a$ is the atmospheric pressure.

Using equation (3), the variable $h$ can be substituted in equation (1), defining the wave speed $c$ as

$$c^2 = \frac{\mathrm{d}p}{\mathrm{d}h} = gh. \tag{5}$$

Equations (1) and (2) can be rewritten, neglecting the diffusion terms, in the form

$$\frac{1}{c^2}\frac{\partial p}{\partial t} + \frac{\partial U_i}{\partial x_i} = 0 \quad (i = 1, 2), \tag{6}$$

$$\frac{\partial U_i}{\partial t} + \frac{\partial F_{ij}}{\partial x_j} + \frac{\partial p}{\partial x_i} + Q_i = 0 \quad (i, j = 1, 2), \tag{7}$$

where the unknowns are now $U_i$ and $p$.

## 3. NUMERICAL PROCEDURE

A time discretization of equations (6) and (7) is introduced to compute changes in $U_i$ and $p$. We thus write

$$\frac{1}{c^2}\frac{\Delta p}{\Delta t} + \frac{\partial U_i^{n+\theta_i}}{\partial x_i} = 0 \tag{8}$$

and, proceeding approximately along the characteristic transport paths[13],

$$\frac{\Delta U_i}{\Delta t} = -\left(\frac{\partial F_{ij}}{\partial x_j} + Q_i\right)^n + \frac{\Delta t}{2}\left[u_k \frac{\partial}{\partial x_k}\left(\frac{\partial F_{ij}}{\partial x_j} + q_i\right)\right]^n - \frac{\partial p^{n+\theta_2}}{\partial x_i} \quad (i, j, k = 1, 2). \tag{9}$$

Here the parameters $\theta_1$ and $\theta_2$ can be chosen in the range 0–1. The first two terms on the right-hand side of equation (9) come from the expansion along the characteristics and the derivation of the equation is illustrated in the Appendix.

By means of this explicit method an appropriate treatment for the convective and source terms of equation (7) can be accomplished, justifying now the use of a Galerkin spatial discretization owing to self-adjointness.

Again based on the discretization along the characteristics, the pressure term in equation (9) can be written as[13]

$$\frac{\partial p^{n+\theta_2}}{\partial x_i} = (1-\theta_2)\frac{\partial p^n}{\partial x_i} + \theta_2 \frac{\partial p^{n+1}}{\partial x_i} - (1-\theta_2)\frac{\Delta t}{2} u_k \frac{\partial}{\partial x_i}\left(\frac{\partial p^n}{\partial x_k}\right) \quad (i, k = 1, 2). \tag{10}$$

In the above

$$U_i^{n+\theta_1} = U_i^n + \theta_1 \Delta U_i, \qquad \Delta U_i = U_i^{n+1} - U_i^n. \tag{11}$$

Inserting equation (11) into (8) and equation (10) into (9), introducing an auxiliary variable $\mathbf{U}^*$ to replace the first two terms on the right-hand side of (9) and observing that $\Delta p = p^{n+1} - p^n$ results in

$$\frac{1}{c^2}\frac{\Delta p}{\Delta t} + \frac{\partial U_i^n}{\partial x_i} + \theta_1 \frac{\partial(\Delta U_i)}{\partial x_i} = 0 \quad (i = 1, 2), \tag{12}$$

$$\frac{\Delta U_i}{\Delta t} = \frac{\Delta U_i^*}{\Delta t} - \frac{\partial p^n}{\partial x_i} - \theta_2 \frac{\partial(\Delta p)}{\partial x_i} + (1 - \theta_2)\frac{\Delta t}{2} u_k \frac{\partial}{\partial x_k}\left(\frac{\partial p^n}{\partial x_i}\right) \quad (i, k = 1, 2). \tag{13}$$

Now $\Delta U_i$ can be eliminated by inserting (13) into (12). The final expression for $p$ is

$$\frac{1}{c^2}\frac{\Delta p}{\Delta t} - \Delta t \theta_1 \theta_2 \frac{\partial}{\partial x_i}\left(\frac{\partial(\Delta p)}{\partial x_i}\right) = -\frac{\partial}{\partial x_i}\left(U_i^n + \theta_1 \Delta U_i^*\right) + \theta_1 \Delta t \frac{\partial}{\partial x_i}\left(\frac{\partial p^n}{\partial x_i}\right) \quad (i = 1, 2), \tag{14}$$

omitting higher-order terms.

Equation (14) is self-adjoint in the variable $\Delta p$ and the standard Galerkin space discretization is again optimal.

The sequence of solution after discretization in space follows the pattern below:

(a) computation of $\Delta U_i^*$
(b) computation of pressure by means of equation (14) and of the new surface elevation using the relation expressed in equation (3)
(c) computation of the final velocity $U_i^n + \Delta U_i$ using equation (13).

Following these steps, this procedure is similar to the fractional step method of Reference 11. However, in the process described above, a splitting of the variables has not been carried out explicitly.

*Space discretization*

For the sake of clarity the three steps are described below in more detail.

(a) Apply the standard Galerkin procedure and the Gauss theorem for the $\Delta U_i^*$ computation, assuming the discretization for the variables as

$$U_i = \mathbf{N}\overline{U}_i;\ \Delta U_i = \mathbf{N}\overline{\Delta U}_i;\ \Delta U_i^* = \mathbf{N}\Delta\overline{U}_i^*;\ q_i = \mathbf{N}\overline{Q}_i$$

(where the overbar denotes the appropriate nodal values). This results in

$$\begin{aligned}\int_\Omega \mathbf{N}^{\mathrm{T}}\mathbf{N}\,\mathrm{d}\Omega \cdot \frac{\overline{\Delta U_i^*}}{\Delta t} = \Bigg[ &-\int_\Omega \mathbf{N}^{\mathrm{T}} u_j \frac{\partial \mathbf{N}}{\partial x_j}\,\mathrm{d}\Omega \cdot \bar{U}_i - \int_\Omega \mathbf{N}^{\mathrm{T}}\mathbf{N}\,\mathrm{d}\Omega \bar{Q}_i \\ &- \frac{\Delta t}{2}\int_\Omega \frac{\partial}{\partial x_k}\left(\mathbf{N}^{\mathrm{T}} u_k\right)\frac{\partial}{\partial x_j}\left(\mathbf{N} u_j\right)\mathrm{d}\Omega \bar{U}_i - \frac{\Delta t}{2}\int_\Omega \frac{\partial}{\partial x_k}\left(\mathbf{N}^{\mathrm{T}} u_k\right)\mathbf{N}\,\mathrm{d}\Omega \bar{Q}_i \\ &+ \frac{\Delta t}{2}\int_\Gamma \mathbf{N}^{\mathrm{T}} u_k \left(\frac{\partial F_{ij}}{\partial x_j} + Q_i\right) \cdot n_k\,\mathrm{d}\Gamma\Bigg]^n,\end{aligned} \tag{15}$$

where all terms on the RHS are computed in the time $n\Delta t = t_n$. Now, introducing the notation

$$\mathbf{M} = \int_\Omega \mathbf{N}^{\mathrm{T}}\mathbf{N}\,\mathrm{d}\Omega, \qquad \mathbf{C} = \int_\Omega \mathbf{N}^{\mathrm{T}} u_j \frac{\partial \mathbf{N}}{\partial x_j}\,\mathrm{d}\Omega, \tag{16}$$

$$\mathbf{K}_u = \int_\Omega \frac{\partial}{\partial x_k}\left(\mathbf{N}^{\mathrm{T}} u_k\right)\frac{\partial}{\partial x_j}\left(\mathbf{N} u_j\right)\mathrm{d}\Omega, \qquad \mathbf{f}_Q = \int_\Omega \frac{\partial}{\partial x_k}\left(\mathbf{N}^{\mathrm{T}} u_k\right)\mathbf{N}\,\mathrm{d}\Omega \bar{Q}_i,$$

the final matrix form of equation (15) is

$$\mathbf{M} \cdot \overline{\Delta \mathbf{U}}^{*} = -\Delta t\left(\mathbf{C}\overline{\mathbf{U}}^{n} + \mathbf{M}\overline{\mathbf{Q}}^{n}\right) - \frac{\Delta t}{2}\left(\mathbf{K}_{u}\overline{\mathbf{U}}^{n} + \mathbf{f}_{Q}\right) + bt1, \tag{17}$$

where $bt1$ represents the last (boundary) term of equation (15) and is identically zero at solid boundaries ($u_n = 0$).

This approximation is conditionally stable and involves only mass matrix inversion for its solution. For one-dimensional problems, neglecting the constraint coming from the source term, the stability condition for pure convection is

$$\Delta t \leq \Delta t_{\text{crit}} = \alpha \frac{h}{|u|}, \tag{18}$$

where $h$ is the element size and $\alpha = 1/\sqrt{3}$ for the consistent mass matrix or $\alpha = 1$ if mass lumping is used. It can be observed that this limit is in terms of the current velocity, instead of the wave velocity as in the Taylor–Galerkin method.[9,15]

When steady state solutions are studied, a local time step defined by (18) is recommended for the right-hand side of (15), giving identical diffusion to that included by the optimal streamline upwinding procedure.[10]

(b) By means of the standard Galerkin method and the discretization

$$p = \mathbf{N}\bar{p}_i, \qquad \Delta p = \mathbf{N}\overline{\Delta p}_i$$

equation (14) leads, after the use of Green's theorem, to the matrix form

$$(\tilde{\mathbf{M}} + \theta_1\theta_2\Delta t\mathbf{H})\Delta\bar{p} = -\Delta t\mathbf{Q}(\overline{\mathbf{U}}^{n} + \theta_1\overline{\Delta\mathbf{U}}^{*}) - \theta_1\Delta t^2\mathbf{H}\bar{\mathbf{p}}^{n} + bt2, \tag{19}$$

where now

$$\tilde{\mathbf{M}} = \int_{\Omega} \frac{1}{c^2}\mathbf{N}^{\mathrm{T}}\mathbf{N}\,\mathrm{d}\Omega, \qquad \mathbf{H} = \int_{\Omega} \frac{\partial \mathbf{N}^{\mathrm{T}}}{\partial x_i}\frac{\partial \mathbf{N}}{\partial x_i}\,\mathrm{d}\Omega,$$
$$\mathbf{Q} = \int_{\Omega} \mathbf{N}^{\mathrm{T}}\frac{\partial \mathbf{N}}{\partial x_i}\,\mathrm{d}\Omega. \tag{20}$$

The boundary terms $bt2$ are

$$br2 = \theta_1\Delta t^2\int_{\Gamma} \mathbf{N}^{\mathrm{T}}\left(\frac{\partial p^{n}}{\partial x_i}\cdot n_i\right)\mathrm{d}\Gamma + \theta_1\theta_2\Delta t^2\int_{\Gamma}\mathbf{N}^{\mathrm{T}}\left(\frac{\partial(\Delta p)}{\partial x_i}\cdot n_i\right)\mathrm{d}\Gamma. \tag{21}$$

The necessary boundary conditions to solve (19) imply the following.

(i) For prescribed elevations in a portion of the boundary both terms of $bt2$ must be computed.

(ii) For totally reflecting wall boundaries the slip boundary condition is imposed for velocities in the solution of both equations (17) and (13). The normal component of (13) to the wall boundary is

$$\frac{\Delta U_i}{\Delta t}\cdot n_i - \frac{\Delta U_i^{*}}{\Delta t}\cdot n_i = -\frac{\partial p^{n+\theta_2}}{\partial x_i}\cdot n_i = 0. \tag{22}$$

Therefore the projection of the approximation to $\partial p^{n+\theta_2}/\partial x_i$ normal to the wall boundary is zero and $bt2$ vanishes.

(c) The final velocity is obtained from the discretization of equation (13), which leads to

$$\mathbf{M}\overline{\Delta\mathbf{U}} = \mathbf{M}\overline{\Delta\mathbf{U}}^{*} - \Delta t\mathbf{Q}\left(\mathbf{p}^{n} + \theta_2\overline{\Delta\mathbf{p}}\right) + \frac{\Delta t^2}{2}\mathbf{P}\bar{\mathbf{p}}^{n}, \tag{23}$$

where

$$\mathbf{P} = (1-\theta_2)\int_{\Omega}\frac{\partial}{\partial x_k}\left(u_k\mathbf{N}^{\mathrm{T}}\right)\frac{\partial \mathbf{N}}{\partial x_i}\,\mathrm{d}\Omega \quad (i,\ k = 1,\ 2).$$

At the completion of this stage the values of $\overline{U}_i$ and $\bar{p}$ at $(n+1)\Delta t$ are fully determined.

It can be observed that if other scalar transport equations are added to the model (e.g. pollutants, temperature), it is only necessary to carry out for them a computation totally analogous to step (a), with the same time step limitation.

*Semi-implicit and explicit forms*

Assuming values of the parameters $\theta_1$ and $\theta_2$ such that

$$\tfrac{1}{2} \leq \theta_1 \leq 1, \qquad \tfrac{1}{2} \leq \theta_2 \leq 1,$$

equation (19) is solved implicitly and the stability limit of the whole solution is governed by the critical time step of equation (18).

Taking $\theta_2 = 0$ (and $\theta_1$ an arbitrary value ($\theta_1 \geq \frac{1}{2}$), e.g. $\theta_1 = \frac{1}{2}$) equation (19) becomes explicit, and calling $\Delta\tilde{t}$ the time step written on the right-hand side, we have

$$\tilde{\mathbf{M}}\frac{\overline{\Delta \mathbf{p}}}{\Delta t} = -\mathbf{Q}\left(\mathbf{U}^n + \theta_1 \overline{\Delta \mathbf{U}}^*\right) - \Delta\tilde{t}\mathbf{H}\mathbf{p}^n + bt2. \tag{24}$$

For stability of solutions the $\Delta t$ on the left-hand side must fulfil the condition[3]

$$\Delta t \leq \frac{h^2}{2c^2\theta_1\Delta\tilde{t}}.$$

The choice of $\Delta\tilde{t}$ is as follows.

(i) $\Delta\tilde{t} = \Delta t$ is necessary for an accurate transient solution. The global stability limit is nearly the same as that for the Taylor–Galerkin method.

(ii) $\Delta\tilde{t} = h/u$: the choice of a local $\Delta\tilde{t}$ gives optimal accuracy for steady state solutions as shown in Reference 10.

## 4. NUMERICAL RESULTS

Some transient and steady state numerical solutions are now considered to illustrate the performance of the algorithm derived here.

### *4.1. Transient solutions*

*Long waves in a rectangular channel.* A rectangular channel is discretized using 40 three-node triangular elements (total 33 nodes). A sinusoidal elevation of amplitude $A = 1$ is prescribed at the left boundary and the rest of the boundary is considered totally reflecting. For a constant depth $H = 5$ m and a channel length $L = 800$ m the critical time step for an explicit Taylor–Galerkin scheme[15] gives $\Delta t \leq 5$ s. In the case of the limit governed by equation (18) the critical time step is $\Delta t \leq 800$ s in terms of the maximum (theoretical) velocity $u = 0{\cdot}102$ m s$^{-1}$ for a monochromatic wave with frequency $\omega = 0{\cdot}005498$ rad s$^{-1}$.

Figures 2(a)–2(c) show the results of the implicit version of the model ($\theta_1 = \theta_2 = 0{\cdot}5$) for the elevations at the extreme right wall point and the velocities at the left free boundary in comparison with the theory. These results were computed for $\Delta t = \Delta t$(explicit) = 5 s, $\Delta t = 50$ s and $\Delta t = 100$ s with very good agreement.

*Annular section with linearly varying depth.* Here a linear depth variation problem with an existing analytical solution is considered. This test was proposed in Reference 16 and is shown in Figure 3(a).

Again a sinusoidal elevation is prescribed at the circular open boundary, considering a frictionless flow. In Figures 3(b) and 3(c) we plot the numerical and theoretical results along a radial direction

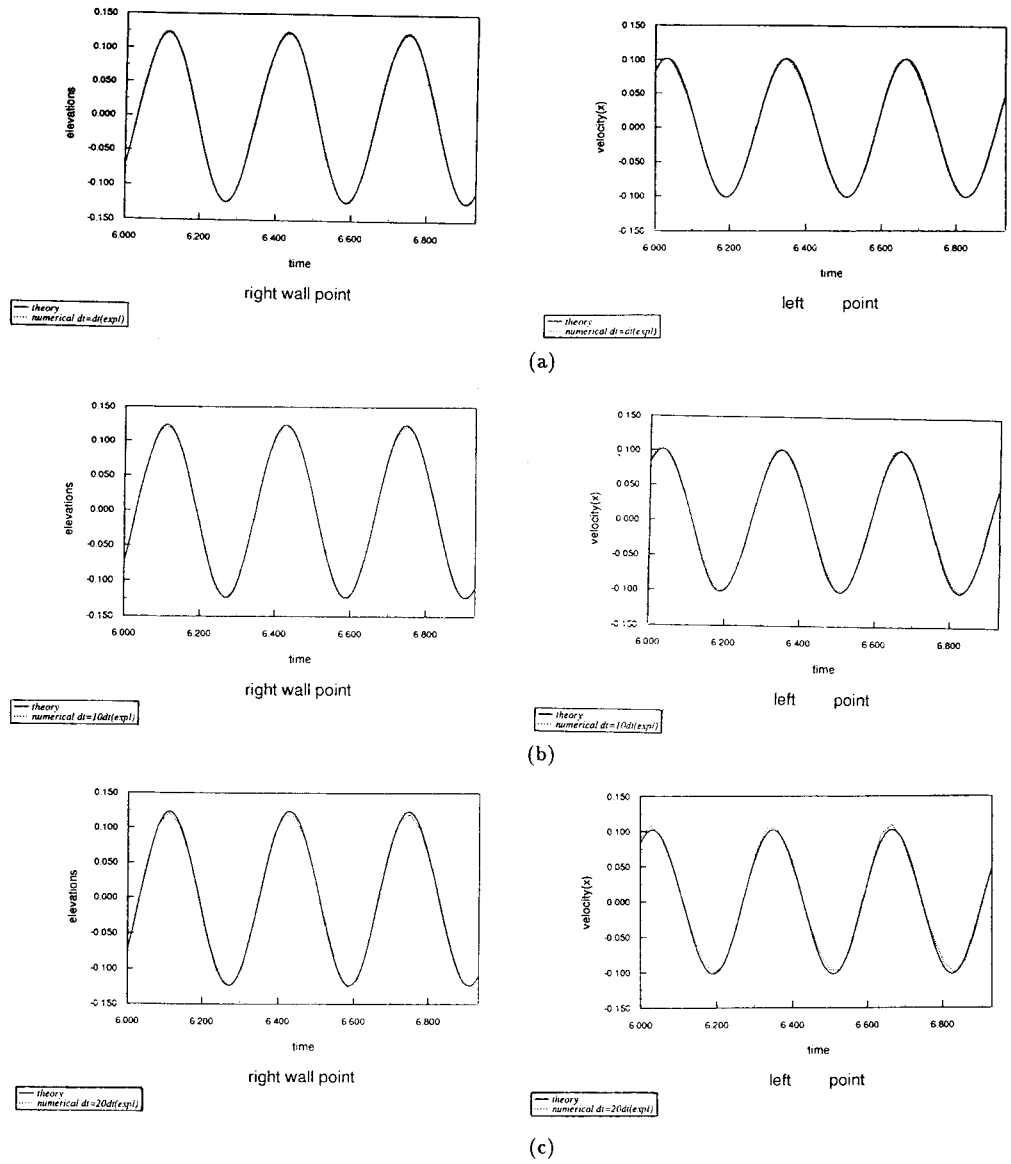


Figure 2. A rectangular channel. Periodic excitation by prescribed input elevation. Results. Semi-explicit model ($\theta_1 = \theta_2 = 0{\cdot}5$) for: (a) $\Delta t = \Delta t$(explicit), (b) $\Delta t = 10\Delta t$(explicit) and (c) $\Delta t = 20\Delta t$(explicit).

($\phi = \pi/4$) for maximum elevation time and maximum velocity time, assuming the following data: $r_1 = 10$ m, $r_2 = 20$ m, $H(r_1) = 10$ m, $H(r) = H(r_1) + r$, $\omega = 0{\cdot}9425$ rad $s^{-1}$.

The results were computed using a triangular mesh with 20 element rows in the radial direction and 10 in the circumferential direction.

A bottom friction term varying from a maximum at $t = 0$ to zero at $t = T$ is included to filter noise. Steady results are reached after two cycles and excellent agreement with the theoretical solution is reached.

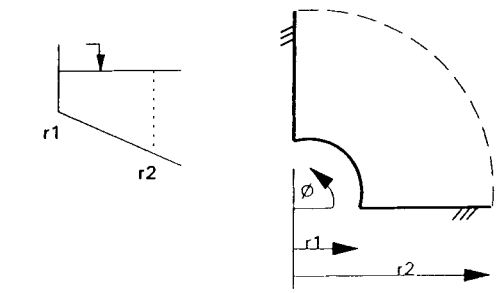


(a)

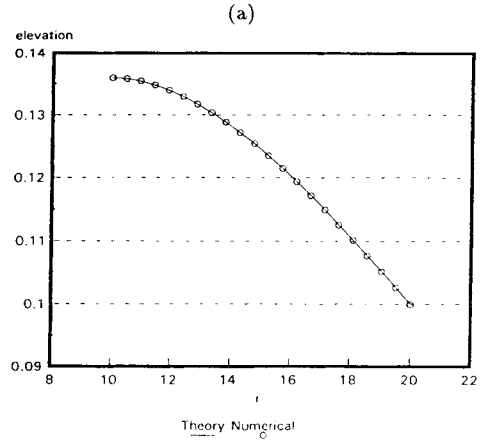


(b)

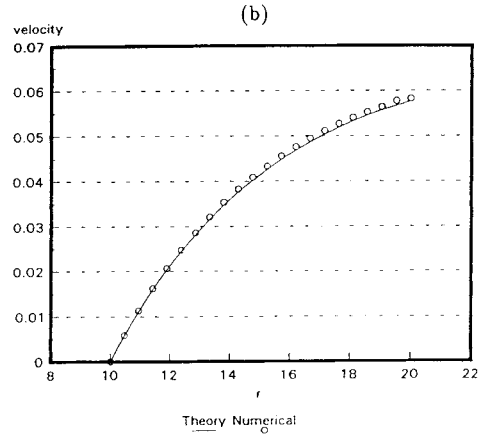


(c)

Figure 3. (a) Annular section with linear varying depth. (b) Maximum elevation $\eta(r)$ at $\phi = \pi/4$. (c) Maximum velocity $v(r)$ at $\phi = \pi/4$

*Severn Estuary.* An application to a real case is presented here. The tidal propagation in the Severn Estuary (Bristol Channel) (Figure 4(a)) is studied with a relatively coarse mesh (Figure 4(b)) of 256 linear triangular elements and 172 points, including full bathymetry description. This is shown in Figure 4(c), where the depth (at mean water level) varies from 40 m at the western limit to less than 10 m at Avonmouth.

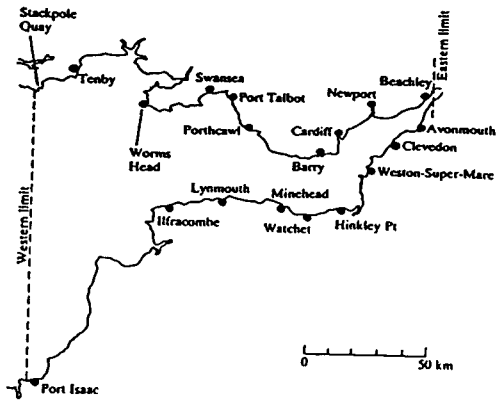


(a)

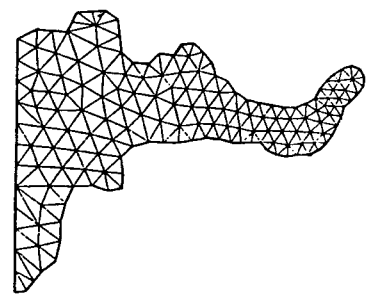

(b)

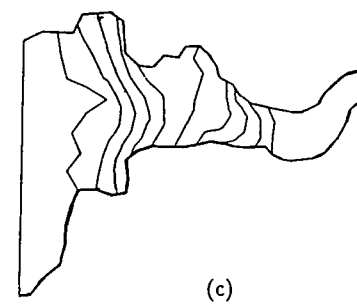

(c)

Figure 4. (a) Severn Estuary. (b) Mesh. (c) Bathymetry ($\Delta h$ = 3 m)

The bottom friction is approximated using a Manning coefficient $n = 0{\cdot}04$.

Stable results are reached after two periods from a 'cold' start and are presented in Figure 5 for the period $T = 12{\cdot}5$ h.

For Figure 5 four control points are chosen: Swansea Bay, Weston-super-Mare, Avonmouth and an exterior boundary point at the centre of the western limit, where a sinusoidal imput elevation is prescribed as 3·65 m tidal amplitude.

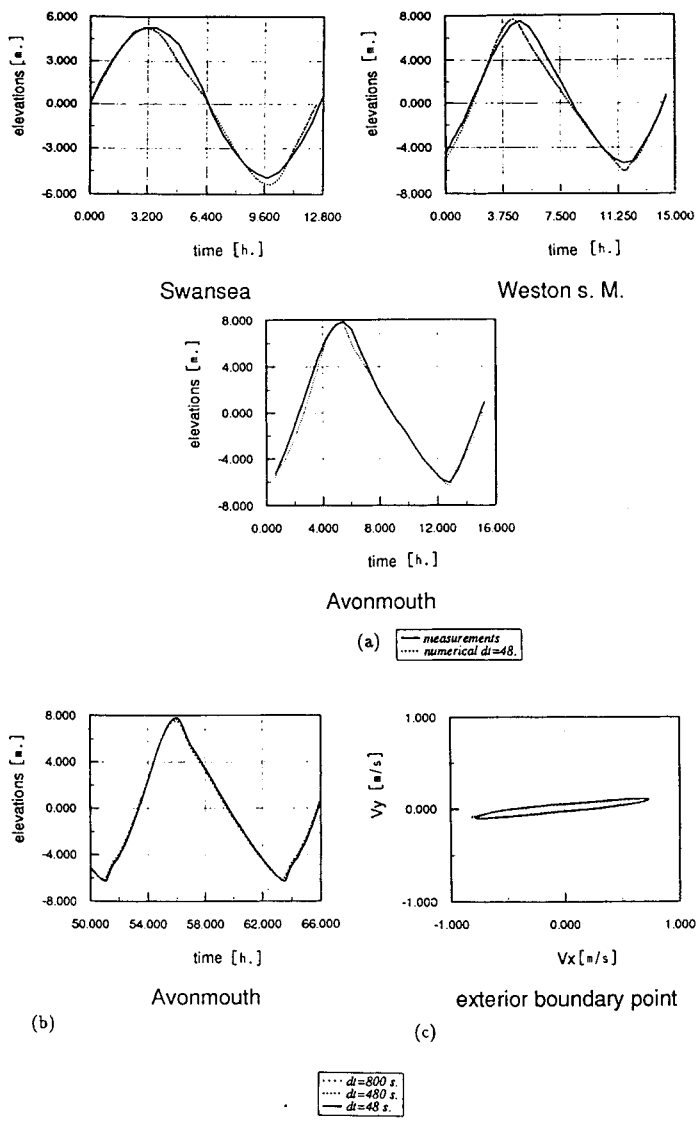


Figure 5. Severn Estuary. (a) Elevations (computed for $\Delta t = 48$ s against measurements). (b) Computed elevations for $\Delta t = 48$ s, $\Delta t = 480$ s and $\Delta t = 800$ s. (c) Exterior boundary point. Computed velocity for $\Delta t = 48$ s, $\Delta t = 480$ s and $\Delta t = 800$ s.

The critical time step for explicit computation is $\Delta t \approx 48$ s and the semi-explicit model has been applied for $\Delta t = \Delta t$(explicit) = 48 s, $\Delta t = 10\Delta t$(explicit) and $\Delta t \approx 17\Delta t$(explicit) with $\theta_1 = \theta_2 = 0{\cdot}5$. In Figure 5(a) the results for $\Delta t = 48$ s are compared at three points with measurements (elevations),[17] showing only slight differences.

The good agreement is retained upon increasing the time step to $16\Delta t$(explicit), as shown in Figure 5(b) for the elevations at the control point of Avonmouth.

The exterior boundary point is chosen to check the velocity results, which are depicted in the phase diagram of Figure 5(c), showing good phase and amplitude behaviour for $\Delta t = 10\Delta t$(explicit) and $\Delta t \approx 17\Delta t$(explicit) in comparison with the results obtained for $\Delta t = \Delta t$(explicit).

The prescribed elevations are imposed at the boundary in Figure 4(a) labelled 'western limit'.

*Tidal bore in the River Severn.* Bore formation is a typically non-linear effect originated by tidal motion and consists of a body of water propagating up a river with the incoming tide, possessing a well-defined front separating it from the slowly ebbing water into which it advances.

The bore moving up the River Severn has been extensively observed and studied (see e.g. Reference 18). In this work an approximation to this phenomenon up from the eastern limit of the Severn Estuary (schematically represented in Figure 6(a) from Avonmouth (A) to Gloucester (G)) is made by an extended mesh obtained by adding 225 elements and 227 nodes to the mesh used in the previous case. A simplified straight mesh was adopted for this prolongation (Figure 6(b)).

A linear depth variation is assumed from $H = 10$ m at Avonmouth (point A of Figure 6(b)) to $H = -6$ m at point G of Figure 6(b), where the distance from A along the river is 77,500 m. The width varies from 6000 m at A to 400 m at B (Blakeney), 200 m at E (Epney) and 30 m at the right extreme and the Manning coefficient considered is 0·04. The measurement points are located at B and E, where the distances from A along the river are 34,000 and 57,500 m respectively.

The semi-explicit model has been applied with $\Delta t = 4\Delta t(\text{explicit}) = 100$ s and the same elevation input as in the previous case has been imposed, along with a steady river flow. The results are depicted in Figure 6(c) for points B and E, where a typical shape of water elevation–time variation for a tidal bore can be observed for point E.

The agreement of the results with the measurements[17] at point B is good (Figure 6(d)), while the differences obtained at point E (Figure 6(e)) are probably due to the simplified bathymetry and geometry adopted.

### *4.2. Steady state solutions—supercritical flow*

Obviously the algorithm can be used to obtain efficient steady state solutions for many shallow water problems. Here we illustrate this type of application for three problems of water flow at supercritical velocities ($F > 1$). These are (i) a boundary wall constriction over one side of an otherwise unbounded flow,[19] (ii) cross-waves formed by a symmetrical wall constriction in a rectangular channel and (iii) a combination of cross-waves and 'negative' jumps in a variable width channel.

These cases pose strong requirements on the performance of the model because of their 'shock'-type solution.

In these problems the vertical accelerations in the vicinity of the jumps are not considered (since a hydrostatic pressure distribution is assumed in the depth integration).

*Boundary wall constrictions.* When the change in the alignment turns towards the centre of a channel as represented in Figure 7(a), a standing wave pattern is created of the type shown in Figure 7(b).

A regular triangular mesh was used (Figure 7(c)) with 2066 nodes and 3955 elements to capture accurately the 'jump' formed.

A comparison is made here between the results obtained by the Taylor–Galerkin method, the new method introduced and the theoretical result.[19]

In Figure 8(a) we plot the contours of elevations for the Taylor–Galerkin method and in Figure 8(b) for the new method, showing a smaller dispersion of the latter for $F_1$ (Froude number of the inflow) = 2·5. In both cases the angle of the shock is close to the theory:

| Theory | Taylor–Galerkin | New |
|---|---|---|
| 39·58° | 39·7° | 39·7° |

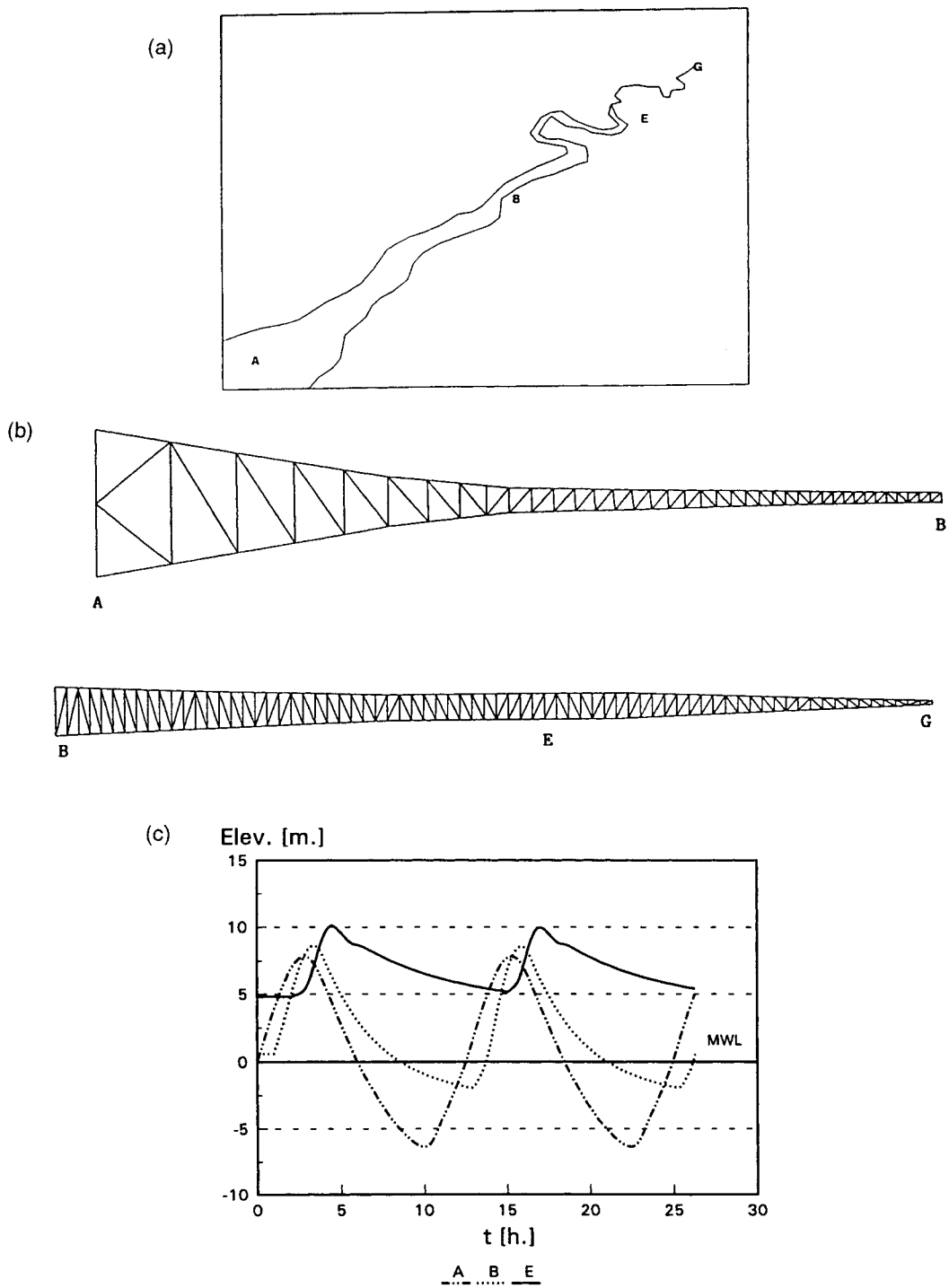


Figure 6. Severn Bore. (a) Severn River from: A (Avonmouth) to G (Gloucester). Measurements points: B (Blackeney), E (Epney). (b) Straight mesh from: A to B (vertical scale = horizontal scale), B to G (vertical scale = 5 × horizontal scale). (c) Water surface elevations history for points A, B, E of (a). Semi-explicit model. (d) Computed and measured elevations of point B. (e) Computed and measured elevations of point E.

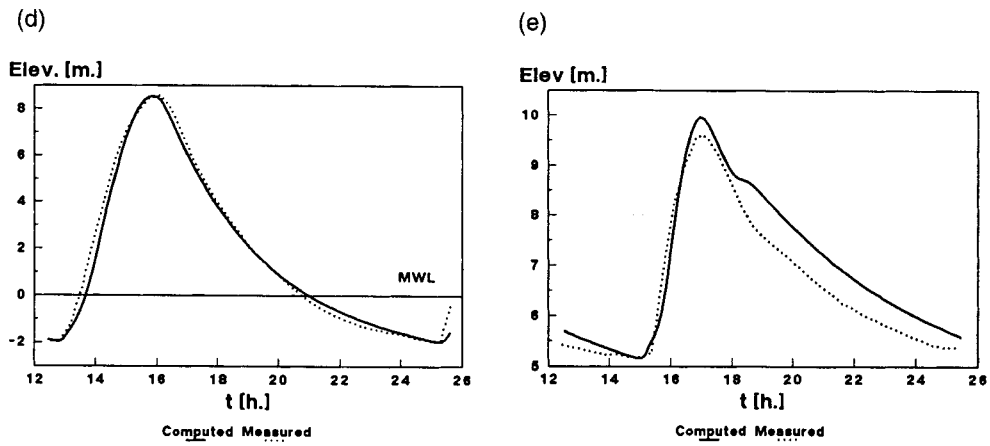


Figure 6 (d), (e)

However, more oscillations are observed with the Taylor–Galerkin method. This can be better seen in Figures 9(a) and 9(b) for the total height and Froude number along the bottom line in comparison with the theory.

No artificial or bottom friction was included, but the interior damping was increased by using a limiting value of $\Delta\tilde{t}$ in the new algorithm.

The better behaviour of the new algorithm is also confirmed when the problem is studied for $F$(inflow) = 3, where fewer oscillations are again observed (Figures 10(a), Taylor–Galerkin; Figure 10(b), new; Figures 11(a) and 11(b)). Now the angles of the shock are:

| Theory | Taylor–Galerkin | New |
|---|---|---|
| 34·36° | 34·5° | 34·4° |

Again no artificial diffusion is required.

The boundary conditions imposed are height and velocities prescribed at the inflow boundary (left boundary), slip boundary condition at the wall, free variables at the outflow (right boundary) and symmetric boundary condition on the upper boundary.

An explicit ($\theta_1 = 0{\cdot}5$, $\theta_2 = 0$) solution was adopted and local time stepping with $\Delta\tilde{t} = h/u$ and a lumped mass matrix was used.

*Symmetric channel constrictions.* If the change in the alignment described above appears on both sides of the channel, a 'cross-wave' pattern is developed.

Considering symmetrical constriction ($\beta = 5°$), a fine regular mesh (Figure 12) of 9181 nodes and 17,975 elements was generated.

The results, presented in Figure 13, are for $h$ = 1 m in region 1 give the following depths:

| Region | Theory ($h$) | Numerical ($h$) |
|---|---|---|
| 2 | 1·254 | 1·25 |
| 3 | 1·55 | 1·54 |

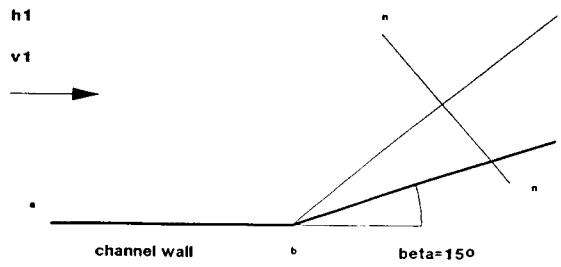


(a)

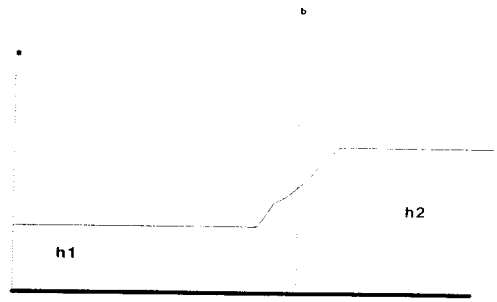


Section n-n

(b)

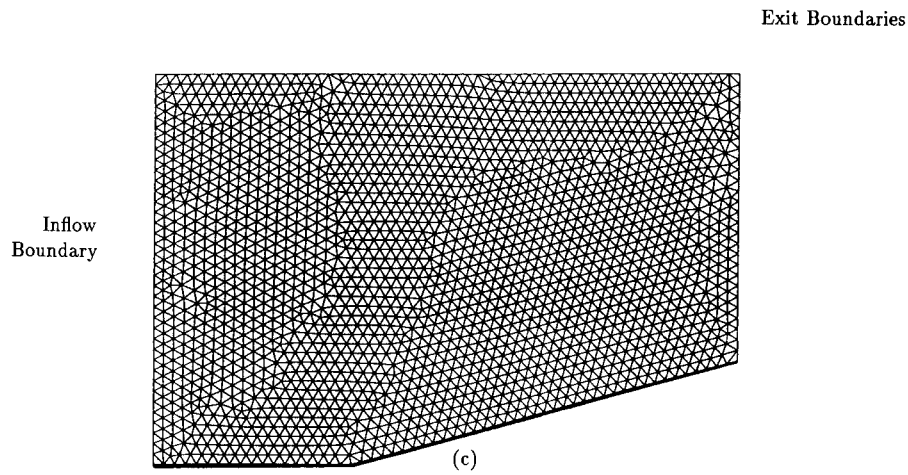


(c)

Figure 7. (a) Problem of boundary wall constriction in supercritical flow. (b) Section of the jump formed. (c) Mesh

These can easily be improved by an adaptive remeshing methodology.[20]

The boundary conditions for this problem are supercritical inflow at the left boundary ($h$, $u_i$ prescribed), free variables at the outflow (right boundary) and slip wall boundary at the sides. The inflow Froude number was taken as 2·5.

The explicit version ($\theta_1 = 0{\cdot}5$, $\theta_2 = 0$) with a lumped mass matrix and local time stepping (in terms of curent velocity) was again used.

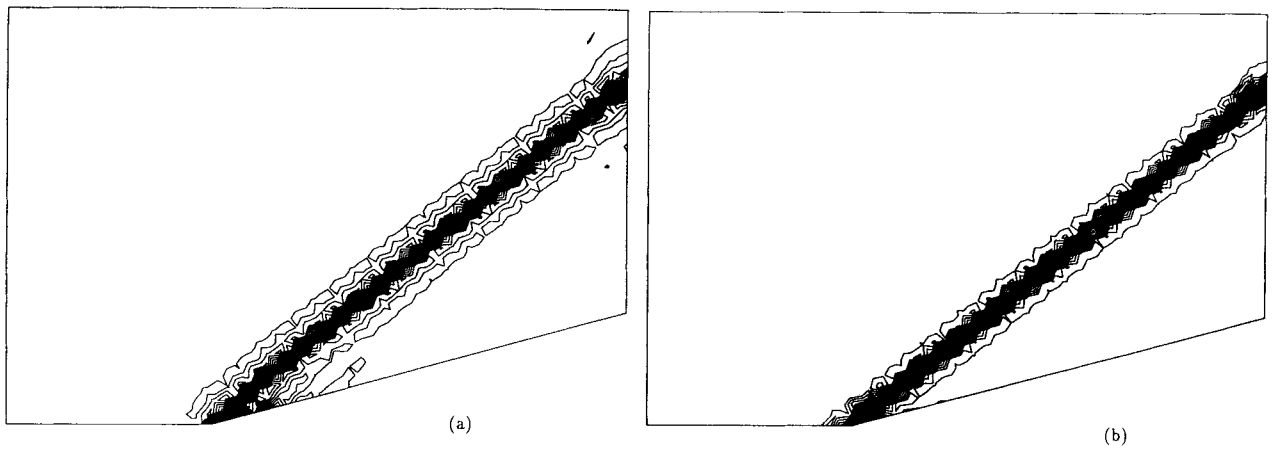


Figure 8. Problem of boundary wall constriction. Froude number 2·5 (inflow). Contours of $h$: (a) Taylor–Galerkin; (b) new algorithm

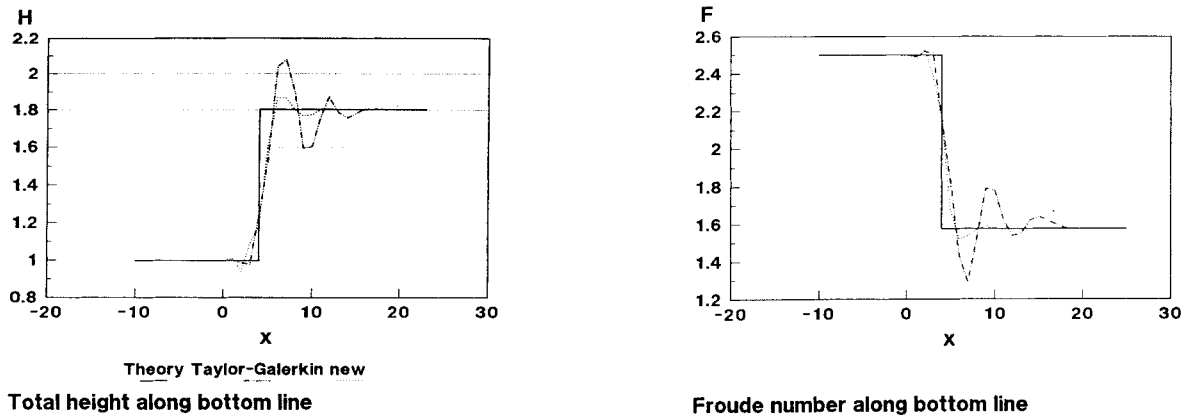


Figure 9. Problem of boundary wall constriction. Froude number 2·5

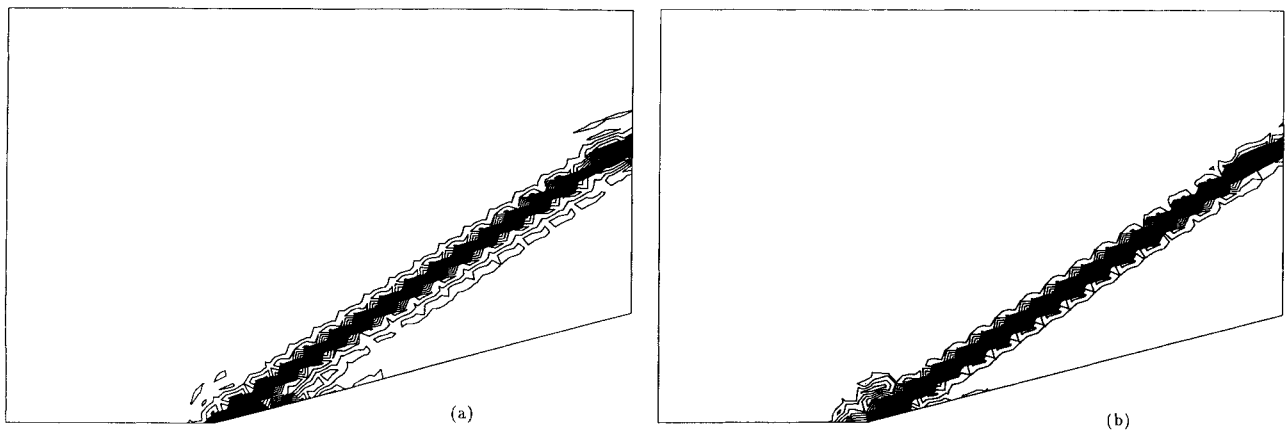


Figure 10. Problem of boundary wall constriction. Froude number 3 (inflow). Contours of $h$: (a) Taylor–Galerkin (b) new algorithm

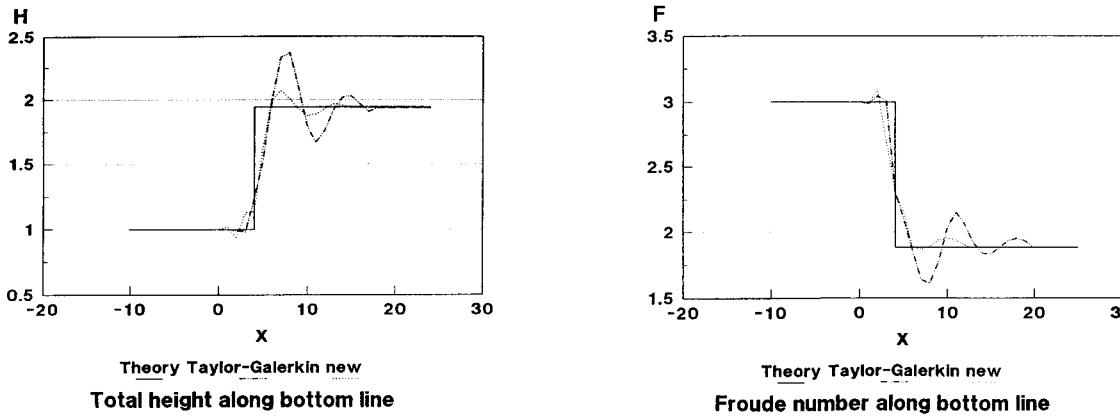


Figure 11. Problem of boundary wall constriction. Froude number 3

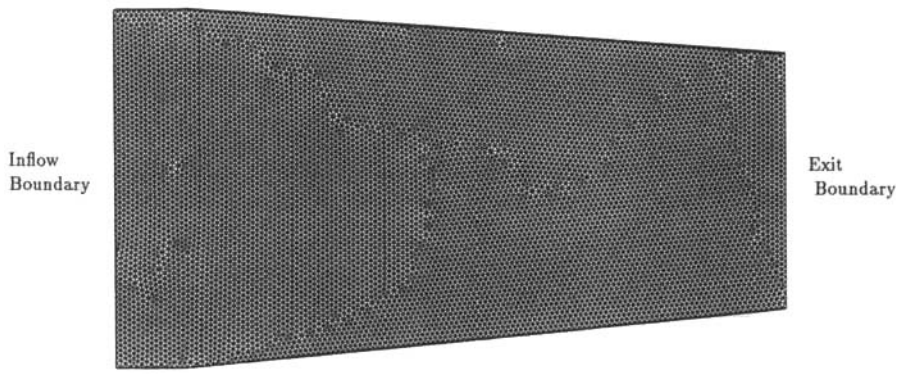


Figure 12. Symmetric channel constriction. Mesh

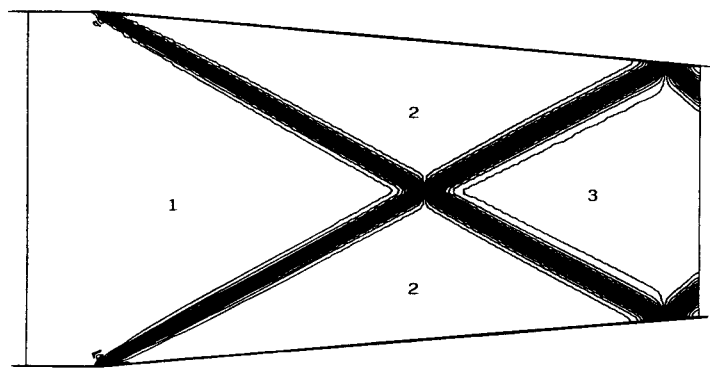


Figure 13. Symmetric channel constriction. Contours of $h$

*Symmetric channel of variable width.* For a supercritical flow in a rectangular channel with a transition of the form shown in Figure 14, a combination of a 'positive' jump, as in the previous example, and 'negative' waves, causing a decrease in depth, appears. The profile of the latter is gradual and an approximate solution can be obtained by assuming no energy losses and that the flow near the wall turns without separation.

Here we study a constriction and enlargement of 15°. The mesh involved has 9790 nodes and 19,151 elements.

Applying the same boundary conditions and version of the model as in the previous example, the final results containing 'cross'-waves and 'negative' waves are represented in Figure 15 (heights). One can observe the 'gradual' change in the behaviour of the negative wave created at the origin of the wall enlargement. Finally, in Figure 16 heights at the wall boundary are plotted, showing that the negative jump at the origin of the enlargement still has a 'shock' characteristic.

## 5. CONCLUSIONS

The new method outlined here represents an improvement over the algorithm presented in Reference 3. Here the introduction of diffusion by means of the 'characteristic–Galerkin' approach is simpler and more direct.

The accuracy is demonstrated in several examples throughout the range of flows encountered in shallow water problems.

A suitable choice of explicit or semi-explicit versions of the model makes it very efficient in the solution of transient and steady state problems. The extension to deal with transport equations can be straightforwardly solved.

Future developments are being focused on the solution of 'drying' area problems, where the geometry of estuarine flows changes, and the inclusion of the vertical distribution of the flow in problems such as tidal and wind-driven circulation.

ACKNOWLEDGEMENT

Dr. Pablo Ortiz is grateful to DGYCIT (Ministerio de Educación y Ciencia, Spain) for the fellowship which permitted him the stay at University College of Swansea (Institute of Numerical Methods in Engineering) in 1993.

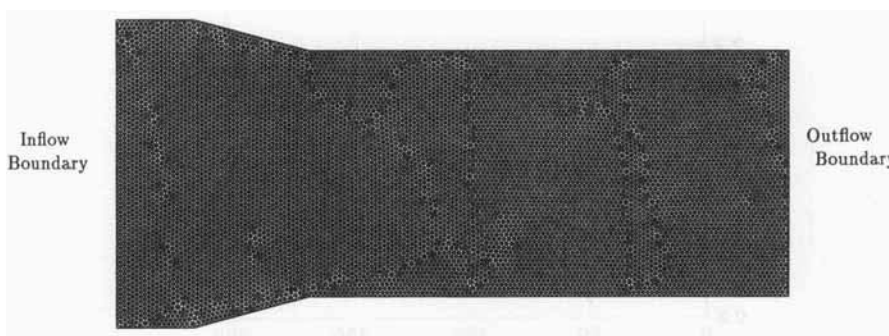


Figure 14. Symmetric channel of variable width. Mesh

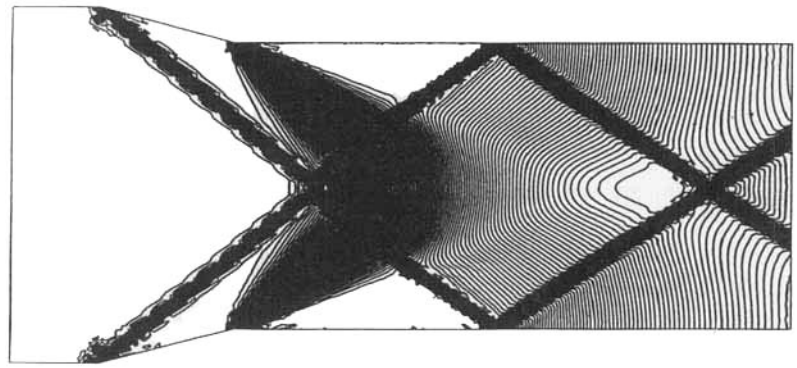

Figure 15. Symmetric channel of variable width. Contours of $h$

## APPENDIX

Consider for simplicity the transport equation of a scalar variable $\phi$ without diffusion,

$$\frac{\partial \phi}{\partial t} + \frac{\partial F_j}{\partial x_j} + Q = 0,$$

where $F_j = u_j \phi$ and $Q$ is a source term.

This can be written as

$$\frac{\partial \phi}{\partial t} + u_j \frac{\partial \phi}{\partial x_j} + \phi \frac{\partial u_j}{\partial x_j} + Q = 0. \tag{25}$$

Calling $\bar{\phi}^n$ the value at $n\Delta t$ at the position $x_i - \delta_i$ (origin of the characteristic, as can be seen in Figure 17 for the space co-ordinate $x_i$), along the characteristic we can write

$$\phi^{n+1} - \bar{\phi}^n = -\Delta t \left( \bar{Q} + \overline{\phi \frac{\partial u_j}{\partial x_j}} \right)^n, \tag{26}$$

where the overbar denotes values which are some average along the characteristic at $x_i$.

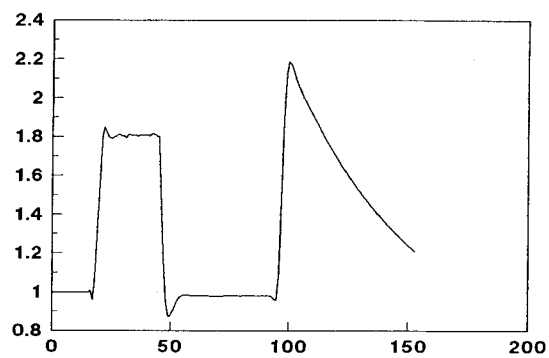


Figure 16. Symmetric channel of variable width. Height along side boundary (m)

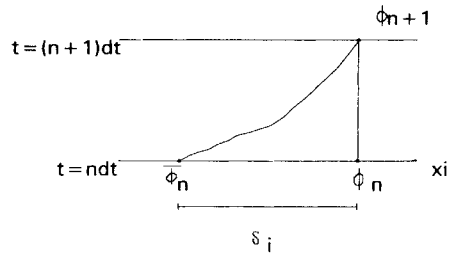


Figure 17. Schematic representation of the characteristic variables

The distance $\delta_i$ can be approximated as

$$\delta_i \approx \Delta t\left(u_i - \frac{\Delta t}{2} u_j \frac{\partial u_i}{\partial x_j}\right)^n.$$

Further, approximating $\bar{\phi}^n$ as

$$\bar{\phi}^n = \phi^n - \delta_i \frac{\partial \phi}{\partial x_i}\bigg|^n + \frac{\delta_i \delta_j}{2} \frac{\partial^2 \phi}{\partial x_i \partial x_j}\bigg|^n$$

and inserting the approximation for $\delta_i$, we can write (omitting terms higher than $\Delta t^2$)

$$\bar{\phi}^n = \phi^n - u_i \Delta t \frac{\partial \phi}{\partial x_i}\bigg|^n + \frac{\Delta t^2}{2} u_j \frac{\partial u_i}{\partial x_j} \frac{\partial \phi}{\partial x_i}\bigg|^n + \frac{\Delta t^2}{2} u_i u_j \frac{\partial^2 \phi}{\partial x_i \partial x_j}\bigg|^n. \tag{27}$$

The evaluation of $\bar{Q}$ and $\overline{\phi(\partial u_j/\partial x_j)}$ in (26) gives

$$\bar{Q} = Q^n - u_i \frac{\Delta t}{2} \frac{\partial Q}{\partial x_i}\bigg|^n, \tag{28}$$

$$\overline{\phi \frac{\partial u_j}{\partial x_j}} = \left(\phi \frac{\partial u_j}{\partial x_j}\right)^n - u_i \frac{\Delta t}{2} \frac{\partial}{\partial x_i}\left(\phi \frac{\partial u_j}{\partial x_j}\right)^n. \tag{29}$$

Now, substituting (27)–(29) into (26), calling $\Delta\phi = \phi^{n+1} - \phi^n$ and reordering, we can obtain

$$\Delta\phi = -\Delta t\left(\frac{\partial F_i}{\partial x_i} + Q\right)^n + \frac{\Delta t^2}{2}\left[u_i \frac{\partial}{\partial x_i}\left(\frac{\partial F_j}{\partial x_j} + Q\right)\right]^n.$$

It can be noted that the final expression does not now include the term $\overline{\phi(\partial u_j/\partial x_j)}$. (For a more detailed derivation see Reference 13.)

## REFERENCES

1. D. R. Lynch and W. Gray, 'A wave equation model for finite element tidal computations', *Comput. Fluids*, **7**, 207–228 (1979).
2. J. Peraire, O. C. Zienkiewicz and K. Morgan, 'Shallow water problems. A general explicit formulation', *Int. j. numer. methods eng.*, **22**, 547–574 (1986).
3. O. C. Zienkiewicz, J. Wu and J. Peraire, 'A new semi-implicit or explicit algorithm for shallow water equations', *Math. Mod. Sci. Comput.*, **1**, 31–49 (1993).
4. M. Kawahara, H. Hirano, K. Tsuhora and K. Iwagaki, 'Selective lumping finite element method for shallow water flow', *Int. j. numer. methods eng*, **2**, 99–112 (1982).
5. O. Daubert, J. Hervouet and A. Jami, 'Description of some numerical tools for solving incompressible turbulent and free surface flows', *Int. j. numer. methods eng.*, **27**, 3–20 (1989).
6. M. G. Foreman, 'An analysis of the 'wave equation' model for finite element tidal computation', *J. Comput. Phys.*, **52**, 290–312 (1983).
7. I. Kinnmark and W. Gray, 'An implicit wave equation model for the shallow water equations', *Adv. Water Resources*, **7**, 168–171 (1984).

8. I. M. Navon, 'A review of finite element methods for solving the shallow water equations', in B. Schreffler and O. C. Zienkiewicz (eds), *Computer Modelling in Ocean Engineering*, Balkema, Rotterdam, 1988, pp. 273–278.
9. J. Donea, 'A Taylor–Galerkin method for convective transport problems,', *Int. j. numer. methods eng.*, **20**, 101–109 (1984).
10. O. C. Zienkiewicz and R. Taylor, *The Finite Element Method*, Vol. 2, McGraw-Hill, (1991).
11. A. J. Chorin, 'Numerical solution of the Navier–Stokes equations', *Math. Comput.*, **22**, 745–762 (1968).
12. C. B. Jiang and M. Kawahara, 'A three-step finite element method for unsteady incompressible flows', *Comput. Mech.*, **11**, 355–370 (1993).
13. O. C. Zienkiewicz and R. Codina, 'A general algorithm for compressible and incompressible flows. Part I: The split characteristic based scheme', *Int. j. numer. methods, fluids,* **20**, 869–885 (1995).
14. O. C. Zienkiewicz and J. Wu, 'A general explicit or semi-explicit algorithm for compressible and incompressible flows', *Int. j. numer. methods eng.*, **35**, 457–479 (1992).
15. J. Peraire, 'A finite element method for convection dominated flows', *Ph.D. Thesis*, University College of Swansea, 1986.
16. D. R. Lynch and W. Gray, 'Analytic solutions for computer flow model testing', *Proc. A.S.C.Y., ASCE*, **104**, HY10, 1400–1428 (1978).
17. B. Allen, University College of Swansea, personal communication, 1993.
18. R. A. Tricker, *Bores, Breakers, Waves and Wakes*, Elsevier, New York, 1964.
19. A. T. Ippen, 'High velocity flow in open channels: symposium', *Trans. ASCE*, **V**, 116 (1951).
20. J. Peraire, . M. Vahadati, K. Morgan and O. C. Zienkiewicz, 'Adaptive remeshing for compressible flow computations', *J. Comput. Phys.*, **72**, 449–466 (1987).